SF2A 2011
G. Alecian, K. Belkacem, R. Samadi and D. Valls-Gabaud (eds)

LYMAN HORIZONS IN THE EARLY PHASES OF THE EPOCH OF REIONIZATION

P. Vonlanthen[1] and B. Semelin[1,2]

Abstract. It has been shown that the radial profile of the Lyman-α flux around light sources emitting in the Lyman band during the early phases of the epoch of reionization is characterized by a series of step-like discontinuities. This property originates in the fact that the neutral intergalactic medium is optically thick at the frequencies of all the Lyman-series lines. We show that, through unsaturated Wouthuysen-Field coupling, these spherical discontinuities are also present in the redshifted 21 cm signal of neutral hydrogen. We use realistic 3D numerical simulations with full radiative transfer calculation in the first five Lyman lines in order to study the properties of these discontinuities and the possibility for detection with the future Square Kilometre Array. Although challenging, these observations could provide a diagnostic tool to disentangle the cosmological signal and residuals from imperfect foreground removal.

Keywords: Radiative transfer, intergalactic medium, large-scale structure of Universe, dark ages, reionization

1 The 21 cm signal

The epoch of reionization is the period in the history of our universe during which the neutral intergalactic medium underwent a major phase transition and became progressively ionized under the influence of the first light sources. This epoch is constrained by a few number of observations only and its most promising probe is the future observation of the redshifted 21 cm line corresponding to the transition between the two hyperfine levels of the HI electronic ground state. The differential brightness temperature of this signal, compared to the cosmic microwave background (CMB), is determined by the following expression (see e.g. Madau et al. 1997; Ciardi & Madau 2003):

$$\delta T_{\rm b} = 28.1\ x_{\rm HI}\ (1+\delta) \left(\frac{1+z}{10}\right)^{1/2} \frac{T_{\rm s}-T_\gamma}{T_{\rm s}} \left(\frac{\Omega_{\rm b}}{0.042}\frac{h}{0.73}\right) \left(\frac{0.24}{\Omega_{\rm m}}\right)^{1/2} \left(\frac{1-Y_{\rm p}}{1-0.248}\right) {\rm mK}, \tag{1.1}$$

where $x_{\rm HI}$ is the neutral hydrogen fraction, $(1+\delta)$ the fractional baryon overdensity at redshift z, T_γ the CMB temperature, and $T_{\rm s}$ the spin temperature, which is related to the ratio of the densities of HI atoms in the two hyperfine levels. $\Omega_{\rm b}$, $\Omega_{\rm m}$, h, and $Y_{\rm p}$ denote the usual cosmological parameters. From that equation, we clearly see that observations of the line are only possible when the spin temperature is different from the CMB temperature. Three processes can excite the hyperfine levels: absorption of CMB photons, collisions, and the Wouthuysen-Field effect. The latter is a radiative coupling mechanism which mixes the two hyperfine levels through absorption and reemission of Lyα photons (Wouthuysen 1952; Field 1958). Thus, the spin temperature can be written as

$$T_{\rm s}^{-1} = \frac{T_\gamma^{-1} + x_\alpha (T_{\rm c}^{\rm eff})^{-1} + x_{\rm c} T_{\rm k}^{-1}}{1 + x_\alpha + x_{\rm c}}, \tag{1.2}$$

where $T_{\rm c}^{\rm eff}$ is the effective color temperature of the UV radiation field, $T_{\rm k}$ the gas kinetic temperature, x_α the coupling coefficient for Lyα pumping, and $x_{\rm c}$ the coupling coefficient for collisions. Once the first radiation

[1] LERMA, Observatoire de Paris, 61 av. de l'Observatoire, 75014 Paris, France
[2] Université Pierre et Marie Curie, 4 Place Jules Janssen, 92195 Meudon Cedex, France

sources appear, the Wouthuysen-Field mechanism is the dominant effect likely to decouple the spin temperature and the CMB temperature. In relation with the local Lyα flux, x_α can be written as

$$x_\alpha = \frac{16\pi^2 T_\star e^2 f_\alpha}{27 A_{10} T_\gamma m_\mathrm{e} c} S_\alpha J_\alpha, \tag{1.3}$$

with e the electron charge, f_α the Lyα oscillator strength, $A_{10} = 2.85 \times 10^{-15}$ s^{-1} the spontaneous emission factor of the 21 cm transition, m_e the electronic mass, c the speed of light and J_α the angle-averaged specific intensity of Lyα photons by photon number. $T_\star = h\nu_{10}/k_\mathrm{B} = 0.0682$ K is the temperature corresponding to the energy difference between the two hyperfine levels, with h the Planck constant, $\nu_{10} = 1420.4057$ MHz the hyperfine transition frequency and k_B the Boltzmann constant. Finally, the backreaction factor S_α accounts for spectral distortions near the Lyα resonance that are caused by recoils and spin diffusivity.

2 Goal of the study

Our goal is to study the role of higher-order Lyman-series photons in the determination of the differential brightness temperature of the 21 cm signal of HI. We are motivated by the fact that the local Lyα photon intensity around primordial sources is made of two contributions (Hirata 2006; Pritchard & Furlanetto 2006):

1. Photons emitted below the Lyβ frequency that redshift to the Lyα frequency as they propagate in the intergalactic medium (IGM);

2. Photons emitted between Lyβ and the Lyman limit that redshift until they reach the nearest Lyman resonance. Because the IGM is optically thick to all the Lyman lines, these photons are absorbed. The subsequent radiative cascades have a given probability to end with the emission of extra Lyα photons.

As a consequence, the radial profile of the Lyα flux around sources emitting in the Lyman band shows a series of steps at the positions of the so-called Lyman horizons, i.e. at distances from the source where photons emitted just below the Ly$(n+1)$ frequency reach the Lyn frequency. Because of the Wouthuysen-Field effect, similar structures appear in the redshifted 21 cm signal. We perform realistic numerical simulations including hydrodynamics and 3D radiative transfer of both ionizing and Lyman band photons, using the code LICORICE (Semelin et al. 2007; Baek et al. 2009; Iliev et al. 2009). The simulated volumes have a minimum size of 100 h^{-1} comoving Mpc. We take into account the first five Lyman-series lines and include the backreaction effect using the simple analytical fit from Hirata (2006). We consider here purely stellar sources (no X-rays), characterized by a Salpeter IMF with masses in the range 1-120 $\mathrm{M}_\odot$.

3 Lyman horizons

We clearly detect Lyman horizons in the early phases of our simulations. As an example, Fig. 1 shows a map of the quantity* $(-\delta T_\mathrm{b} \times r^2)$ at $z = 13.42$, with r the distance to the source center, in arbitrary units (Vonlanthen et al. 2011). The source (white spot) is the first to light up at $z = 14.06$ in a 100 h^{-1} comoving Mpc simulation. The Lyϵ, Lyδ and Lyγ horizons are marked with white, yellow and red arrows respectively. The slice thickness is 2 h^{-1} comoving Mpc and the colorscale is logarithmic. Note that there is no Lyβ horizon. Indeed, because of quantum selection rules, a Lyβ photon cannot produce a Lyα photon. The sizes of the horizons can be precisely computed. In the redshifts of interest for this study ($z \approx 14-10$), the result is in the range 50-59 comoving Mpc for the Lyγ discontinuity, 27-31 comoving Mpc for Lyδ, and 16-19 comoving Mpc for Lyϵ, assuming standard values for the cosmological parameters.

Furthermore, we find that detection of these features are seriously affected by the appearance of other nearby sources. This is illustrated in the left panel of Fig. 2, in which we plot the gradient of the spherically averaged δT_b profile around the same source as in Fig. 1. The four panels show the profile at different redshifts, from $z = 13.22$ to $z = 11.64$. At early times, Lyman horizons are detected as peaks in the δT_b gradient at the predicted positions (indicated by arrows). But as more and more sources light up, fluctuations in the Lyα background around individual sources appear, which translates into similar fluctuations in the 21 cm signal. We find that the Lyϵ and Lyδ discontinuities can be detected during an interval $\Delta z \sim 2$ after the first source

*As δT_b is approximately proportional to r^{-2}, mapping the product of the differential brightness temperature and r^2 will straighten up the radial profiles and improve visualization.

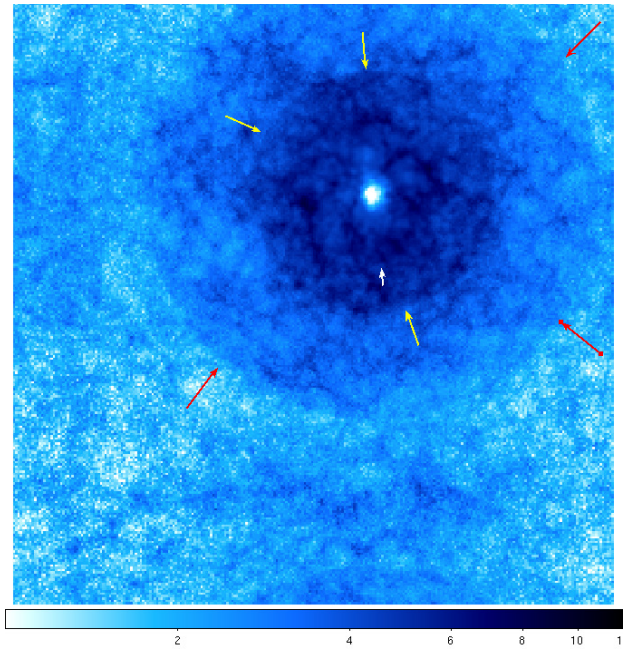

Fig. 1. Map of the quantity $-\delta T_\mathrm{b} \times r^2$ at $z = 13.42$, with r the distance to the source center, in arbitrary units. We indicate the positions of the Lyϵ, Lyδ and Lyγ horizons with white, yellow and red arrows respectively.

lights up, with temperature jumps in the range 2-4 mK. The Lyγ horizon is weaker and is observable during an interval $\Delta z < 1.5$ only.

Stacking all the individual profiles inside the simulation box at a given redshift allows us to extend the detectability period for the Lyδ and Lyϵ horizons to $\Delta z \sim 4$, that is for $10 < z < 14$ in our simulations.

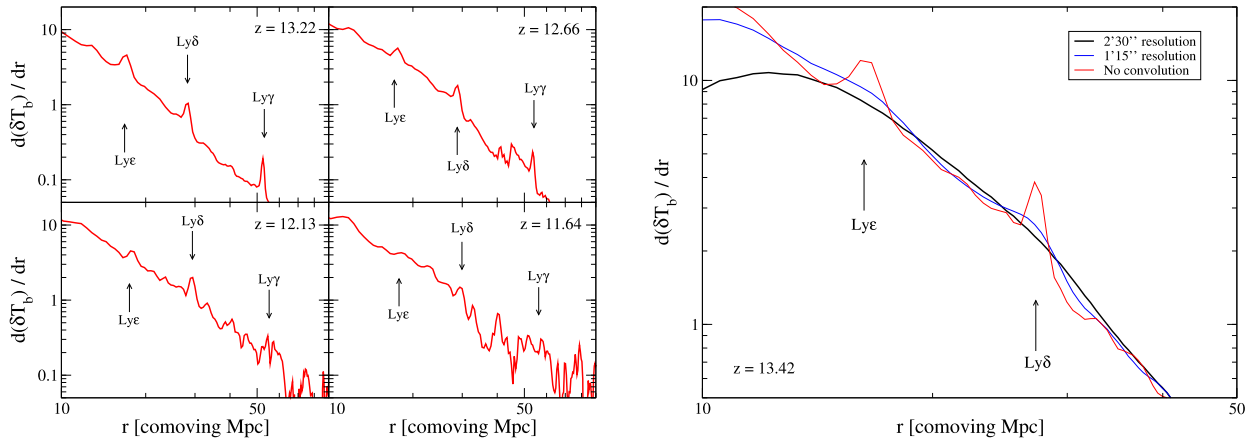

Fig. 2. Left: Gradient of the spherically averaged profile of the differential brightness temperature, around the same source as in Fig. 1. The four panels show the profile at different redshifts. Arrows indicate the predicted positions of the first three horizons. **Right:** The thick black line shows the gradient of the δT_b stacked profile in a 200 h^{-1} comoving Mpc simulation at $z = 13.42$, with SKA-like noise, assuming a field of view of 400 deg^2, and a $2'30''$resolution. The horizons are wiped off by the limited SKA resolution. The blue line assumes an optimistic $1'15''$resolution. The red line shows, for comparison, the gradient of the profile without noise nor resolution effect.

4 Detection with the Square Kilometre Array?

Detection of these distinctive rings in the future 21 cm observations would be of great interest for people involved in the very difficult task of foreground removal. Indeed, these structures of known sizes at a given redshift could provide a diagnostic tool for the cosmological origin of the detected signal after removal procedures.

For that reason, we investigated the possibility for detection with the planned Square Kilometre Array (SKA). In order to do so, we included in our simulated data the effect of both SKA noise and resolution. The effect of noise can be softened if we consider a large field of view (several hundreds of square degrees) and stacking of the radial profiles around sources. The most limiting factor will probably be the limited resolution of the instrument. Indeed, assuming the currently favored design, the 5-km core translates into a resolution between $2'$ and $3'$ in the range $10 < z < 14$. The right panel of Fig. 2 shows that such a resolution completely erases the Lyman horizons (black line). However, if we optimistically assume a resolution that is twice better (corresponding to a 10-km core), then the Lyδ horizon can be observed as a wide and weak hump (blue line).

We conclude from this figure that detection of the Lyman horizons in the early phases of the epoch of reionization using the SKA will be a challenging task. It could be possible for the Lyδ horizon with a resolution of the order of one arcminute.

This work was realized in the context of the LIDAU project. The LIDAU project is financed by a French ANR (Agence Nationale de la Recherche) funding (ANR-09-BLAN-0030). PV acknowledges support from a Swiss National Science Foundation (SNSF) post-doctoral fellowship. This work was performed using HPC resources from GENCI-[CINES/IDRIS] (Grant 2011-[x2011046667]).

References

Baek, S., Di Matteo, P., Semelin, B., Combes, F., & Revaz, Y. 2009, A&A, 495, 389

Ciardi, B. & Madau, P. 2003, ApJ, 596, 1

Field, G. B. 1958, Proc. I. R. E., 46, 240

Hirata, C. M. 2006, MNRAS, 367, 259

Iliev, I. T., Whalen, D., Mellema, G., et al. 2009, MNRAS, 400, 1283

Madau, P., Meiksin, A., & Rees, M. J. 1997, ApJ, 475, 429

Pritchard, J. R. & Furlanetto, S. R. 2006, MNRAS, 367, 1057

Semelin, B., Combes, F., & Baek, S. 2007, A&A, 474, 365

Vonlanthen, P., Semelin, B., Baek, S., & Revaz, Y. 2011, A&A, 532, A97

Wouthuysen, S. A. 1952, AJ, 57, 31